GEOPHYSICS, VOL. 72, NO. 1 (JANUARY-FEBRUARY 2007); P. C9–C17, 14 FIGS., 7 TABLES.
10.1190/1.2392817

42235.

AVO as a fluid indicator: A physical modeling study

Aaron Wandler[1], Brian Evans[2], and Curtis Link[1]

ABSTRACT

Information on time-lapse changes in seismic amplitude variation with offset (AVO) from a reservoir can be used to optimize production. We designed a scaled physical model experiment to study the AVO response of mixtures of brine, oil, and carbon dioxide at pressures of 0, 1.03, and 2.07 MPa. The small changes in density and velocity for each fluid because of increasing pressure were not detectable and were assumed to lie within the error of the experiment. However, AVO analysis was able to detect changes in the elastic properties between fluids that contained oil and those that did not. When the AVO response was plotted in the AVO intercept-gradient domain, fluids containing oil were clearly separated from fluids not containing oil. This was observed in the AVO response from both the top and base of the fluids in the physical model. We then compared the measured AVO response with the theoretical AVO response given by the Zoeppritz equations. The measured and theoretical AVO intercept responses for the top fluid reflection agree well, although the AVO gradients disagree slightly. For the fluid base reflection, the measured and theoretical responses are in close agreement.

INTRODUCTION

The characteristics of seismic reflection, particularly amplitude variation with increasing offset, can identify changes in elastic properties useful for discriminating lithology types and identifying pore fluids. Using a physical modeling approach, we are able to distinguish between fluid-only mixtures containing oil from non-oil fluid mixtures using amplitude variation with offset (AVO) intercept-gradient analysis. Our fluid mixtures were combinations of water, brine, oil, and carbon dioxide. Even though water and oil can have similar acoustic properties and are the most difficult systems for observing seismic differences (Lumley, 2001), our physical modeling investigation distinguishes fluid types based on relatively small changes in velocity and density. For a comprehensive review and tutorial of AVO analysis, see Castagna (1993).

Characterizing the reflection response of a fluid, whether liquid or gas, has been a topic of much interest. Rutherford and Williams (1989) group gas-sand reflection responses into three classes based on their AVO characteristics and defined them in terms of normal incidence for the top of the gas-sand reflection. Foster and Keys (1999) investigate the effects of elastic rock properties on AVO response in the AVO slope-AVO intercept domain. They compare the change in reflection from the tops and bases of sands containing gas or light hydrocarbons and examined how pore fluid compressibility affects AVO response.

AVO response can change significantly due to variations in hydrocarbon properties. For example, changes in fluid phase caused by reservoir production can significantly change the seismic response from a reservoir (Batzle et al., 1995). Batzle et al. (2001) suggest the change in elastic moduli caused by changes in fluid saturation can be extracted from seismic data, in terms of a direct indicator for fluid modulus, and used to indicate pore fluids.

AVO has been used also as a successful tool for reservoir monitoring. Tura and Lumley (1999) show that AVO data can detect changes in fluid saturation resulting from production and Landro (2001) specifically uses near- and far-offset stacked data to observe saturation changes at the top reservoir interface.

Knowing that pore fluid properties can influence reflection response, we investigate how different fluids, in the absence of a rock matrix, affect AVO behavior. We start with pure water and progressively complicate the fluid to one that resembles a reservoir mixture.

We use a physical modeling system to record common-midpoint (CMP) gathers from a model designed to hold fluids at pressures from 0 to 2.07 MPa. An advantage of physical modeling is the precise control achieved for model dimensions and characteristics. Our approach used an acrylic model containing a cell designed for injection of fluid-only mixtures under pressure. Only the fluid mixtures were put under pressure. The fluid-only mixtures were combinations of water, brine, oil, and carbon dioxide (CO_2), and reached equilibri-

Manuscript received by the Editor February 13, 2006; revised manuscript received June 18, 2006; published online December 13, 2006.
[1]Montana Tech, Department of Geophysical Engineering, Butte, Montana 59101. E-mail: aaron.wandler@gmail.com; clink@mtech.edu.
[2]Curtin University, Department of Exploration Geophysics, Perth, Australia. E-mail: brian.evans@geophy.curtin.edu.au.

Table 1. Acoustic properties of materials used to construct the model.

Material	Density (gm/cm³)	V_P (m/s)	V_S (m/s)
Acrylic	1.18–1.19 (Harper, 1975)	2730 (McIntire, 1991)	1430 (McIntire, 1991)
Stainless steel type 347	8.0 (Davis, 1990)	5740 (McIntire, 1991)	3090 (McIntire, 1991)

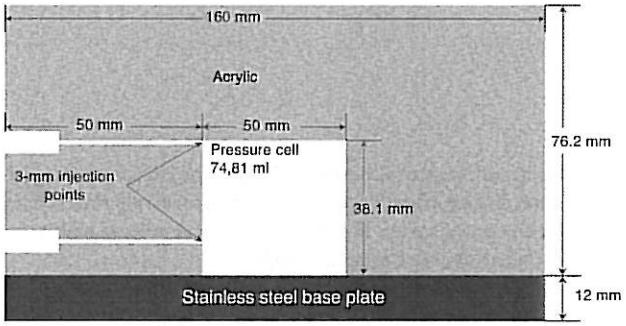

Figure 1. Cross-section view of the physical model. (Drawing not to scale.)

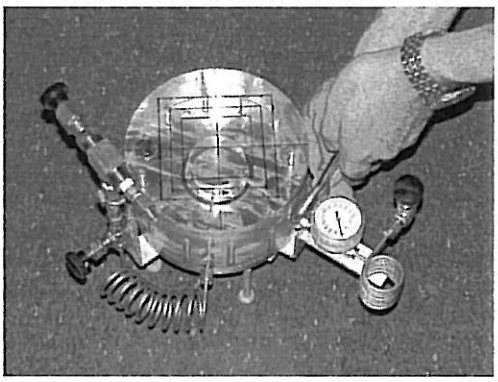

Figure 2. Model assembled with valves and pressure gauge.

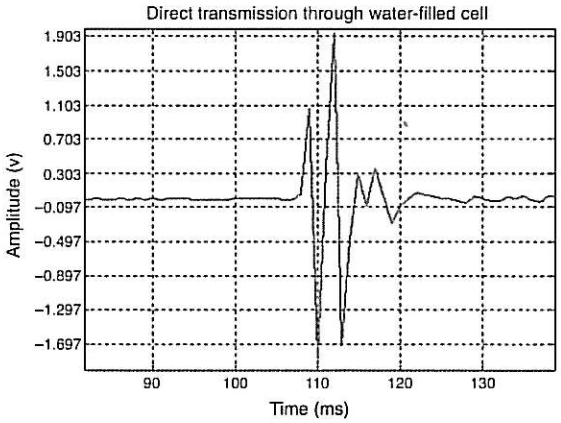

Figure 3. Acoustic signature of the source transducer.

um at the various pressures before data were collected. The model was machined from a solid piece of acrylic (Plexiglas) to create a hollow core for fluid injection. This piece of acrylic was then sealed and bolted to a stainless steel plate. Piezoelectric ultrasonic transducers attached to computer-controlled arms were used for the acoustic source and receiver.

Zoeppritz (1919) formulated the theoretical response of angle-dependent reflectivity from an interface. In our study, we compared the calculated Zoeppritz response with the recorded reflection amplitudes from the acrylic/fluid and fluid/base plate interfaces. The model materials (acrylic and stainless steel) produce a large reflection coefficient at the fluid interface. Therefore, we do not implement any of the various approximations to the Zoeppritz equations that assume angles of incidence and changes in elastic properties at the interface are small.

To analyze the AVO response of the various fluid combinations, we crossplot the AVO attributes' intercept and gradient. AVO intercept and AVO gradient are affected by changes in elastic properties. Crossplotting these attributes highlights even subtle differences related to fluid type.

METHODS

Physical model

We used acrylic and stainless steel, which have well-established properties (Table 1), to construct our physical model. Figure 1 shows a cross section of the model and its dimensions. Figure 2 is a photograph of the model showing its relative size, the components for fluid injection, and the data collection template drawn on the top of the model. The model was designed and tested to withstand an internal pressure of up to 2.76 MPa (400 psi), but experiments were conducted only up to 2.07 MPa (300 psi).

Data acquisition system

Data were collected using Curtin University's physical modeling recording system, described in Evans (2004). A desktop computer controls the movement, firing sequence, and sampling frequency of the ultrasonic piezoelectric transducers that are used as the source and receiver. The transducers are positioned by computer-controlled stepper motors. The data acquisition controller software accepts inputs for the movement, firing sequence, and sampling frequency of the transducers and is implemented in LabView©. The piezoelectric transducers used in this experiment were 1 MHz Panametrics type V103 with a non-semicircular radiation pattern set to a sampling frequency of 10 MHz. The transducers were placed in direct contact with the model and a coupling agent (treacle) was used to maximize energy transmission. Figure 3 shows the acoustic signature of the source transducer.

Fluid mixtures

Five fluid combinations were injected into the model pressure cell under three different pressures: 2.07 MPa (300 psi), 1.03 MPa (150 psi), and 0 MPa (0 psi), at 21 °C, resulting in 30 data sets: 15 zero offset and 15 CMP. Zero-offset and angle-dependent data were recorded at each pressure. Table 2 lists the fluids and their initial pro-

portions prior to injection. The oil was a light, sweet crude with API gravity 37.7 and the CO_2 was obtained from dry ice.

Injection procedure

Prior to injection into the model pressure cell, the fluids were mixed in a 700-ml external cylinder. The process was straightforward for the fluids that did not contain oil. The external cylinder was filled completely with water or water-NaCl then the fluid mixture was injected through the bottom injection point of the model until the pressure cell was completely filled and any trapped air removed. At this time, the valve to the top injection point was closed and a high-pressure hose was attached to the external cylinder. Fluid pressure was increased in the external cylinder and the pressure cell until the desired pressure was obtained. Then the valve to the bottom injection point was closed, leaving the fluid in the cell at the desired pressure.

The procedure for the water-oil mixture was more complicated. Because our supply of crude oil was limited, we could mix only a total volume of 100 ml for injection into the cell (Table 2). We used the same procedure to inject the water-oil mixture into the model pressure cell that was used for water and water-NaCl. We injected approximately a 6:1 mixture of water to oil in the pressure cell by visual inspection.

The fluid preparation for the water-oil-CO_2 and water-NaCl-oil-CO_2 mixtures was similar to that for the water-oil mixture. The only difference was that, when the water and oil (for the water-oil-CO_2 mixture) or water, NaCl, and oil (for water-NaCl-oil-CO_2 mixture) were in the external cylinder, we added CO_2 in solid dry ice form and immediately closed the top valve to the cylinder. We let these mixtures reach equilibrium in the closed cylinder at room temperature for several hours. After the mixtures reached equilibrium, we injected them into the model pressure cell to achieve an approximately 6:1 mixture of water to oil like the nonCO_2 case.

Our experimental apparatus did not allow us to keep the initial amount of CO_2 under enough pressure to remain completely dissolved in the various fluids during the injection process from the pressure cylinder into the physical model's pressure cell. This was problematic because we were unable to determine the exact amount of CO_2 dissolved in the fluid or fluid mixture. Another problem we encountered was the external pressure cylinder was almost empty when CO_2 was added to the water-oil mixtures. This operational difficulty of injecting fluids mixed with oil in an adequate and controlled amount from the external pressure cylinder into the model pressure cell made it difficult to estimate the quantity of CO_2 that was dissolved in the fluid prior to injection into the model. However, we knew CO_2 had been dissolved in the water-oil-CO_2 and water-NaCl-oil-CO_2 mixtures because a gas cap formed when the pressure was reduced from 1.03 to 0 MPa.

Data collection

We collected zero-offset and CMP data for each of the five fluid mixtures at 2.07, 1.03, and 0 MPa, starting with the highest pressure and progressing to lower pressures. Zero-offset data were collected using one transducer as both the source and the receiver. A zero-offset profile for water only at 0 MPa (Figure 4) shows the acoustic response as the transducer stepped across the top of the model from left to right, in increments of 1 mm. The event at approximately 0.056 ms on the far-left and far-right of the section is the reflection from the acrylic/stainless steel base plate interface. The event at 0.028 ms is the reflection from the acrylic/water interface at the top of the cell, while the event at 0.079 ms is the reflection from the water/stainless steel base plate interface at the bottom of the cell. These reflections correlate to the interfaces shown in Figure 1.

CMP data were collected using two transducers — one acting as the source and the other acting as the receiver. The CMP geometry is illustrated in Figure 5 for the top reflection and Figure 6 for the base reflection with offsets ranging from 21.2 to 72.5 mm. Figure 7 shows four CMP gathers recorded with water in the pressure cell at 0 MPa. The gathers were recorded from the center of the pressure cell and the top reflection trough occurs at 0.0284 ms. Figure 8 shows a window containing the base reflection peak of the water/

Table 2. Fluids injected into the pressure cell and their initial proportions.

Fluids	Amount of deionized water (ml)	Amount of NaCl (gm)	Amount of solid (dry ice) CO_2 (gm)	Amount of crude oil (ml)
Water	700			
Water-NaCl	700	21		
Water-oil	70			30
Water-oil-CO_2	70		10	30
Water-NaCl-oil-CO_2	70	2.1	10	30

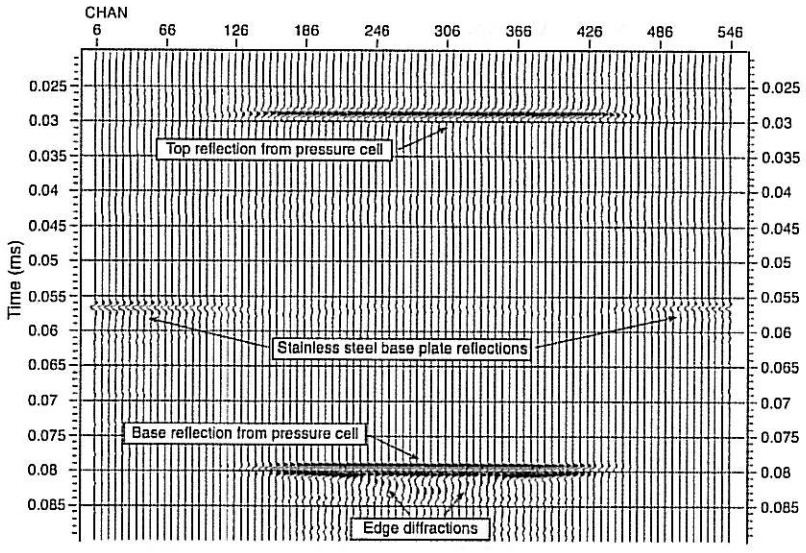

Figure 4. Zero-offset profile over model containing water at 0 MPa in the pressure cell.

stainless steel interface of the four central CMP gathers occurring at 0.0794 ms. We used only the four central CMP gathers so the AVO analysis would not be affected by edge diffractions. Diffractions can be seen on the zero-offset section in Figure 4.

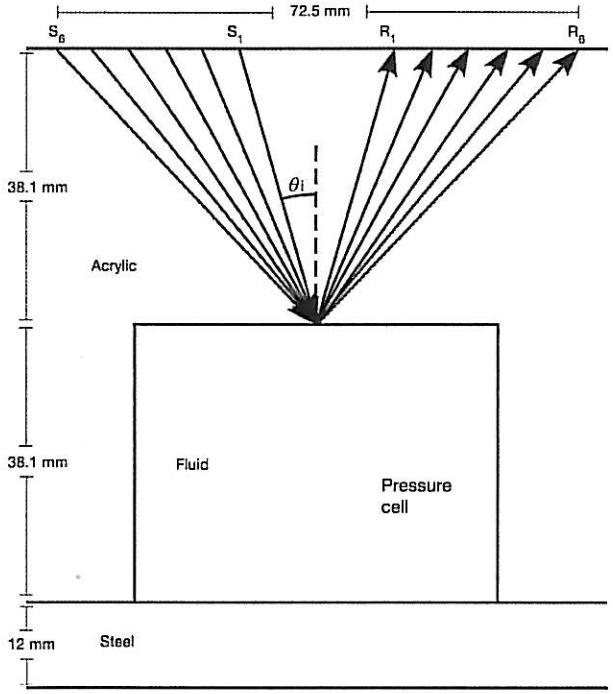

Figure 5. Raypaths for the transducer positions of the top reflection from the acrylic/fluid interface. (Drawing done to scale.)

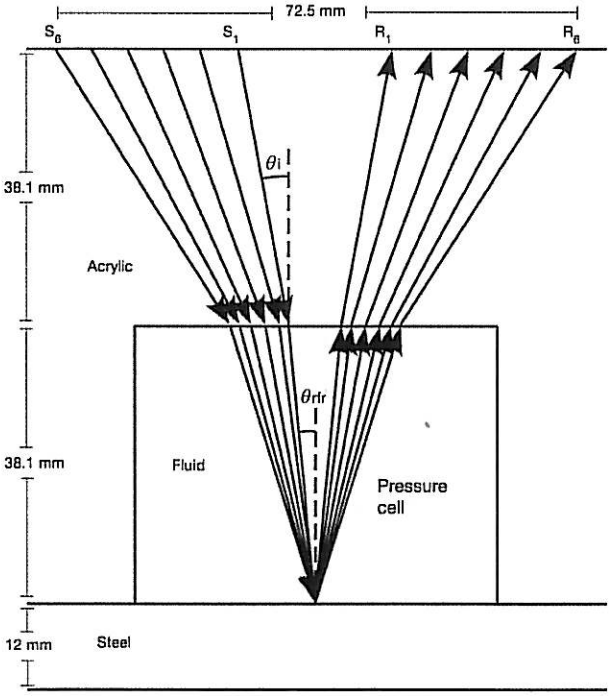

Figure 6. Raypaths for the transducer positions of the base reflections with water at 0 MPa in the pressure cell. (Drawing done to scale.)

Initially, we expected to see reflection response changes caused by changing pressure and fluid type in the zero-offset data. However, the elastic properties of the fluids do not change enough between 2.07 and 0 MPa to produce a noticeable and consistent zero-offset reflection anomaly. We collected data in a CMP configuration to investigate changes in the AVO response to different fluids at different pressures. Again, because the properties of the fluids varied slightly between 2.07 and 0 MPa, we did not observe a consistent change in the AVO response from changes in these pressures. We were able to visually determine the change from dissolved CO_2 to a free gas in the water-oil-CO_2 and the water-NaCl-oil-CO_2 mixtures because, when pressure was reduced from 1.03 to 0 MPa, gas was liberated to form a gas cap at the top of the pressure cell.

Ray tracing

Source-receiver offsets for the CMP gathers are given in Table 3. Figure 5 illustrates the CMP geometry for the six traces recorded for the reflection from the top of the pressure cell. Angles of incidence and reflection are given in Table 4.

To calculate the reflection angles we used a shooting-ray method. Figure 6 illustrates the ray tracing results for the base reflections. The angles of incidence and refraction for each trace for the base reflections from the pressure cell are given also in Table 4. The angles of incidence and refraction for the base of the pressure cell depend on the velocity of the fluid. However, Table 4 only shows the values for water at 0 MPa because neither the angle of incidence nor the angle of refraction changes more than 0.5° for all fluids at the three pressures.

Another approach to transform from offset to angle domain uses the relation derived from the Dix formula (Dix, 1955):

$$\sin\theta = \frac{xv_{int}}{tv_{rms}^2} \qquad (1)$$

Here x is offset, v_{int} is interval velocity for a particular layer, t is total offset traveltime, and v_{rms} is the root-mean-square (rms) velocity to the top of the layer. This approximation is used by the Hampson-Russell software to calculate the AVO intercept and gradient. Table 5 compares the angles obtained by using the shooting-ray method to those from the approximation using equation 1.

Data processing

Processing of the CMP data was minimal to preserve true amplitude. The processing flow before AVO analysis was simply vertical stacking, trace weighting, and normal moveout correction. The only unconventional step in the processing flow is the trace weighting to correct for the transducer radiation pattern. Prior to the experiments, the source and receiver radiation patterns of the transducers were measured so the offset amplitudes could be corrected from a focused signature (Figure 9) to a semicircular signature. The correction factor was calculated by dividing the peak direct transmission amplitude by the actual direct transmission radiation amplitude at the desired angle for both the source and receiver transducers. The individual source and receiver correction factors were multiplied to give a combined source and receiver correction factor. These combined correction factors were then used to correct each CMP-offset trace.

Table 6 lists the values used to correct the corresponding trace of the CMP gather for the top and base reflections to semicircular radiation pattern.

AVO attributes

We used the Hampson-Russell AVO software package for AVO analysis. AVO intercept and gradient values were generated by fitting a line through reflection amplitudes versus $\sin^2(\theta)$, where θ is the incident angle, using statistical methods (Walden, 1991) to minimize the effects of outlying amplitudes on the regression. The intercept represents the normal incidence reflection coefficient and the gradient is the reflection response trend with respect to offset. The AVO intercept was crossplotted against the AVO gradient to highlight any differences related to fluid or pressure.

Modeling

We compared the results of our experiment to numerically modeled results from the Zoeppritz equations using software developed and provided by the Consortium for Reaserch in Elastic Wave Exploration Seismology at the University of Calgary (www.crewes.org). We did not use the methods described by Walden (1991) to calculate the AVO intercept and AVO gradient of the modeled data because the modeled data should be absent of outlying amplitudes.

RESULTS

Velocity estimation

From the zero-offset data, we calculated the velocities of the fluid combinations at the different pressures. We compared our measured values to values given by Batzle and Wang (1992) for some of the fluids (Table 7); we based the standard deviation of the measured velocity on $\frac{1}{2}$ of the sampling frequency. All of our measured velocities are within 0.27% difference of the values given by Batzle and Wang (1992). We then used Batzle and Wang's values to estimate the amount of water and oil contained in the pressure cell. We used a weighted average of the reference values for water and oil velocities to match the measured velocity:

$$v_{mixture} = \phi_{water} v_{water} + \phi_{oil} v_{oil} \quad (2)$$

where ϕ_{water} and ϕ_{oil} are the volume fractions of water and oil, and v_{water} and v_{oil} are the compressional velocities for water and oil. We determined that the water-oil mixture in the pressure cell was approximately 65 ml water and 10 ml oil.

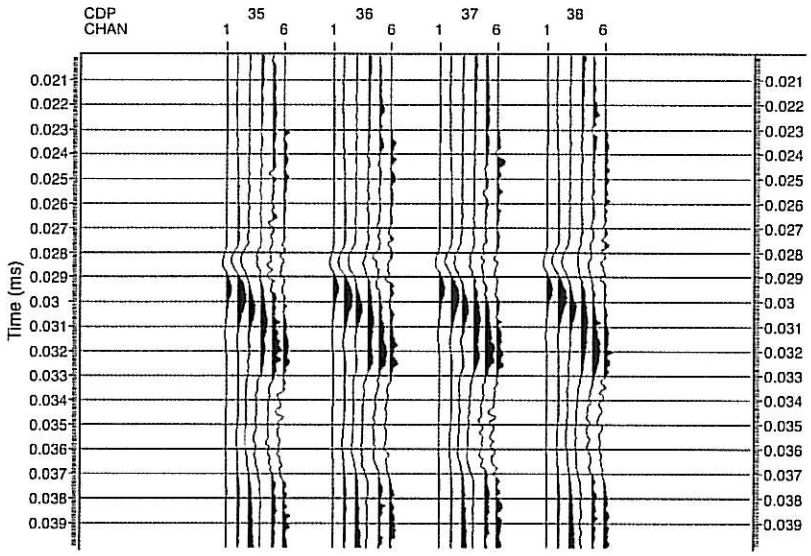

Figure 7. CMP gathers recorded from the center of the pressure cell. The trough of the top reflection from the acrylic/fluid interface is at 0.0284 ms. The fluid in the model was water at 0 MPa.

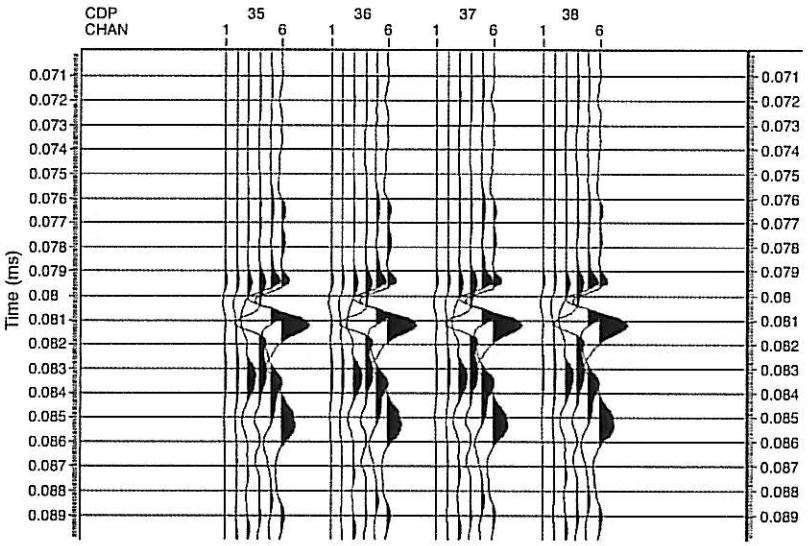

Figure 8. CMP gathers recorded from the center of the pressure cell. The peak of the base reflection is from the fluid/stainless steel interface at 0.0794 ms. The fluid in the model was water at 0 MPa.

Table 3. Range of CMP offsets over top of model.

Trace number	Source-receiver offset (mm)
1	21.2
2	31.5
3	41.7
4	52.0
5	62.3
6	72.5

AVO analysis

To analyze the AVO response of the top reflection, we chose the trough at 0.0284 ms and the four center CMPs that were not affected by edge diffractions (Figure 7). [See the zero-offset profile (Figure 4) that shows the edge diffractions.] For the base reflection, we chose the peak at 0.0794 ms and the four center CMPs (Figure 8). We used only the first four traces because the base reflection in the fifth and sixth traces was beyond the critical angle. After observing that the change in pressure only slightly affects the density and compressional velocity of the fluid (Table 7) and these changes minimally affect the Zoeppritz response, we determined that any change in AVO response caused by pressure was within the experimental error. Based on this observation, the experimental AVO response for each fluid was averaged for the three different pressures.

The theoretical AVO intercept that represents the reflection coefficient at normal incidence lies between −1 and 1. However, the AVO intercepts calculated from the experimental CMP gathers do not lie within the −1 to 1 range because of scaling factors in the recording system.

Table 4. Angles of incidence and reflection for the top and base of the pressure cell containing water at 0 MPa.

	Top of pressure cell	Base of pressure cell	
Trace number	Incident/Reflection angle acrylic/fluid	Incident angle acrylic/fluid	Reflection angle fluid/stainless steel
1	15.5	10.3	5.6
2	22.5	15.0	8.2
3	28.7	19.8	10.7
4	34.3	24.2	13.0
5	39.3	28.7	15.2
6	43.6	32.6	17.2

Table 5. Comparison of reflection angles of incidence between the approximation method and the shooting-ray method for the base reflection of pressure cell containing water at 0 MPa.

	Base of pressure cell		
Trace number	Offset (mm)	Approximation angle of reflection fluid/stainless steel	Shooting ray method angle of reflection fluid/stainless steel
1	21.2	4.7	5.6
2	31.5	7.0	8.2
3	41.7	9.1	10.7
4	52.0	11.3	13.0
5	62.3	13.3	15.2
6	72.5	15.2	17.2

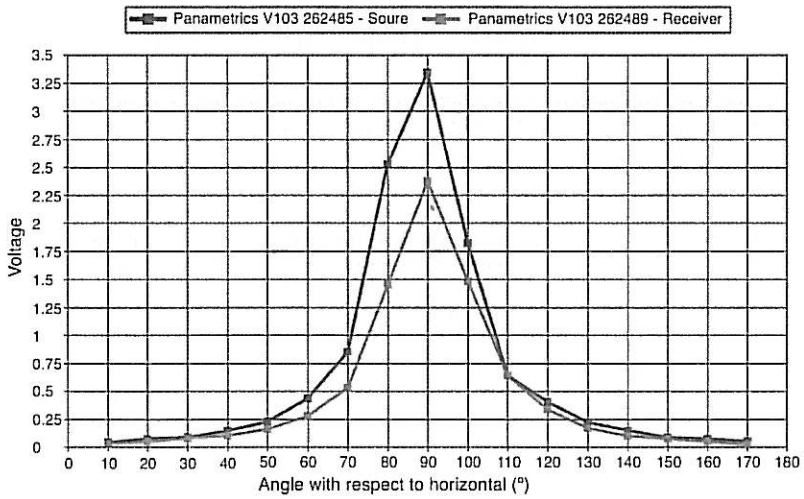

Figure 9. Radiation pattern of the ultrasonic transducers used as seismic source and receiver.

AVO response-top reflection

The crossplot of the AVO intercept and gradient of the reflection from the top of the pressure cell for the five different fluid combinations and the CO_2 gas cap is shown in Figure 10. The error bars in the AVO crossplot are calculated from the averages of the AVO intercepts and gradients at each of the three experimental pressures. The AVO crossplot of the top reflection shows there is a change in response with the addition of oil to water. The fluids without oil form a group separate from the fluids mixed with oil. Figure 10 also compares the AVO response produced by the CO_2 gas cap with the AVO response from the other fluids. The CO_2 gas cap forms at the top of the pressure cell when the CO_2 is liberated from the solution between 1.03 and 0 MPa. Its error bars are calculated from these two responses. The apparent groupings of fluids are quantified by multivariate analysis of variance (MANOVA). Using the results provided by the simultaneous 95% confidence interval, we conclude that there are four different top reflection responses. The first response is the CO_2 gas cap; the second group is water, water-NaCl, and water-oil; the third from water-oil and water-NaCl-oil-CO_2; and the fourth response from water-oil-CO_2 and water-NaCl-oil-CO_2. These four different responses from MANOVA agree with the apparent separation between the fluids shown in Figure 10. (See Johnson, 1998 for a review of MANOVA.)

We also calculated the theoretical Zoeppritz response for the top reflection of the pressure cell for three experimental liquid combinations and the CO_2 gas cap using the fluid densities and velocities from Batzle and Wang (1992) and Lide (2004) (Table 7). Figure 11 shows the theoretical Zoeppritz AVO response to these fluids. We observe that, as fluid density and velocity increase, the AVO intercept and gradient decrease.

AVO response-base reflection

The AVO crossplot from the base reflection for the different experimental fluids clearly shows that the AVO response of oil is distinct from water or brine (Figure 12). The crossplot for the base reflection is clearly separated into two groups: fluids with oil and fluids without oil. We again quantified the apparent grouping of fluids by MANOVA. Using results provided by the simultaneous 95% confidence interval, we conclude the base reflection contains three different groups of responses. The first group is water and water-NaCl, the second is water-oil and water-NaCl-oil-CO_2, and the third is water-oil-CO_2 that has a response different from the other fluids. These three different responses from MANOVA agree with the apparent separation between the fluids in Figure 12. The theoretical Zoeppritz response also suggests that even a small change in average density and velocity can be detected in the AVO response from the base reflection of the pressure cell (Figure 13). Again, as the fluid density and velocity increase, the AVO intercept and gradient decrease.

DISCUSSION OF RESULTS

The AVO crossplot from the top reflection (Figure 10) shows a change in AVO response with the addition of oil and CO_2. Comparing the AVO response of the liquids to the CO_2 gas cap (Figure 10), we see the expected large change in AVO response from the gas. Although there is separation in the AVO responses for water and water-NaCl, compared to the AVO responses for fluids containing a water-oil mixture or a CO_2 gas cap, the AVO responses for mixtures containing oil do not agree completely with the theoretical Zoeppritz responses for the top reflection. The calculated Zoeppritz response shown in Figure 11 shows the AVO intercept and AVO gradient decreasing from water-oil, to water, to water-NaCl. The measured response shows the AVO intercepts for the fluids behave like the trend of the Zoeppritz response; however, the AVO gradient does not. We are unable to explain why this behavior occurs. Given that the AVO intercept and gradients for the top reflection exhibit relatively large experimental error compared to the intercepts and gradients for the

Table 6. Correction factors for spherical radiation pattern amplitude corrections.

Trace number	Correction factor top reflection	Correction factor base reflection
1	4.69	2.22
2	21.4	4.73
3	54.0	15.7
4	93.5	27.3
5	183	50.6
6	267	83.4

Table 7. Calculated velocities from the physical model compared with literature values.

Material or fluid	Calculated density (gm/cm^3) (Batzle and Wang, 1992)	Calculated velocity (m/s) (Batzle andWang, 1992)	Observed velocity (m/s)	Velocity percent difference
Acrylic	1.18–1.19 (Harper, 1975)	2730 (McIntire, 1991)	2732 ± 4.90	0.0732
CO_2 gas	$1.964^{*}10^{-3}$	259 (Lide, 2004)		
Water; 0 MPa	0.996	1497	1497 ± 1.47	0
Water; 1.03 MPa	0.9964	1498	1500 ± 1.48	0.1334
Water; 2.07 MPa	0.9969	1500	1500 ± 1.48	0
Water-NaCl; 0 MPa	1.0164	1528	1530 ± 1.54	0.1308
Water-NaCl 1.03 MPa	1.0169	1530	1533 ± 1.54	0.1959
Water-NaCl 2.07 MPa	1.0174	1531	1533 ± 1.54	0.1305
Water-oil; 0 MPa	0.9747	1477	1479 ± 1.44	0.1353
Water-oil; 1.03 MPa	0.9751	1479	1482 ± 1.44	0.2026
Water-oil; 2.07 MPa	0.9754	1481	1485 ± 1.45	0.2697
Water-oil-CO_2 0 MPa			N/A CO_2 gas cap	
Water-oil-CO_2 1.03 MPa			1488 ± 1.45	
Water-oil-CO_2 2.07 MPa			1488 ± 1.45	
Water-oil-NaCl-CO_2 0 MPa			N/A CO_2 gas cap	
Water-oil-NaCl-CO_2 1.03 MPa			1482 ± 1.44	
Water-oil-NaCl-CO_2 2.07 MPa			1488 ± 1.45	

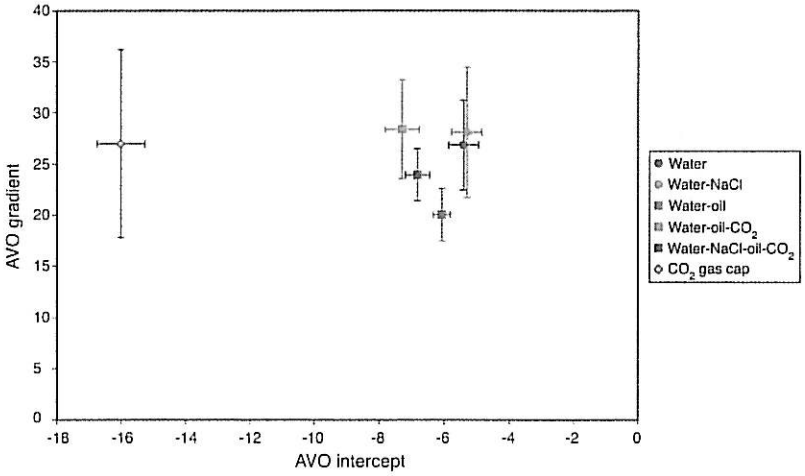

Figure 10. AVO crossplot of the top of pressure cell reflection.

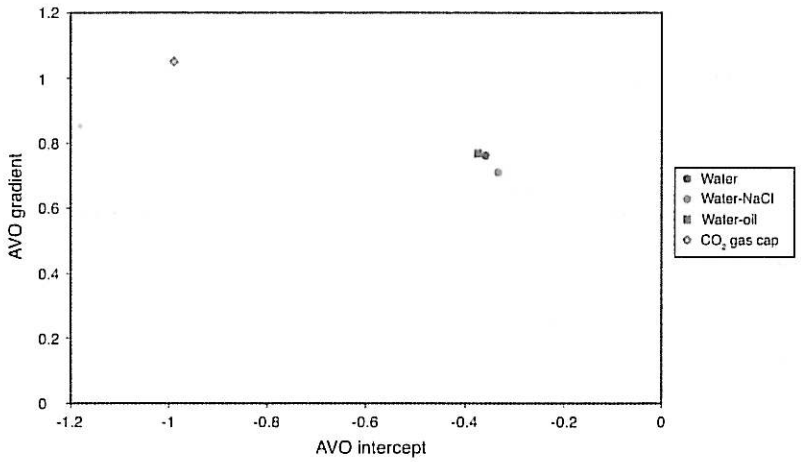

Figure 11. AVO crossplot of theoretical Zoepprtiz response to top of the pressure cell reflection of fluids with known density and velocity.

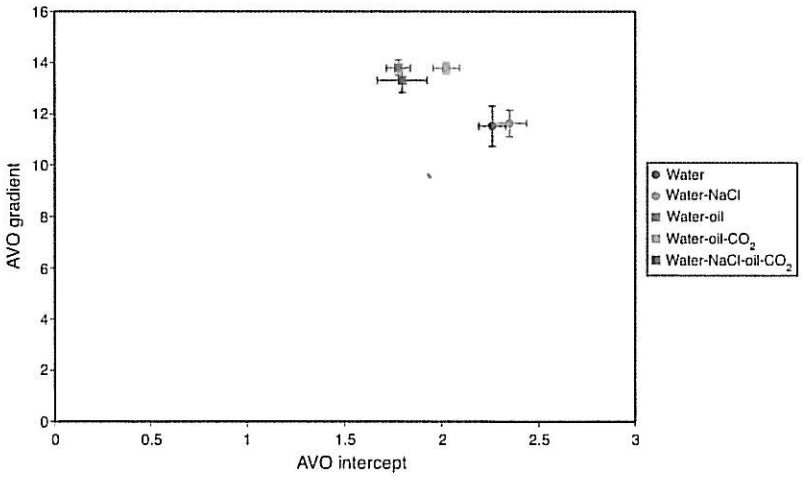

Figure 12. AVO crossplot of the base of pressure cell reflection.

bottom reflection, we surmise that the large error bars from the response of the top reflection of the pressure cell are due to the large angles of incidence.

The AVO crossplot for the base reflection (Figure 12) clearly shows that changes in fluid composition affect the AVO response. Like the AVO response of the top reflection, the base reflection AVO response exhibits a clear separation between water and water-NaCl, and the water-oil mixtures. The calculated Zoeppritz response for the base reflection (Figure 13) shows the AVO intercept decreases very little from water-oil, to water, to water-NaCl, but there is a significant decrease in AVO gradient from water-oil, to water, to water-NaCl.

Unlike the top reflection AVO gradient (Figure 10), the base reflection AVO gradient (Figure 12) agrees with the trend of the AVO gradient in the theoretical Zoeppritz response (Figure 13); however, the base AVO intercept trends do not agree. Again, we are unable to explain why this behavior occurs. It is worth noting that the AVO response from the base reflection (Figure 12) results from a reflection beneath a fluid mixture in which the oil and water are almost completely separated. Thus, the base interface was murky water containing remnant hydrocarbons on stainless steel (Figure 14). Even though most of the water had separated from the oil in water-oil mixtures, the AVO response still responds to the presence of hydrocarbons in the fluid system. This AVO response behavior could have significant implications for reservoir management strategies — especially with fully instrumented oil fields that use steam or water injection to aid recovery. If a bottom reflector of the reservoir could be identified and compared at various stages as the reservoir matures, the change in AVO response could possibly be used to estimate the remaining amount of unproduced oil.

Most of the uncertainty encountered in this experiment came from the injection of fluids from the external pressure cylinder into the physical model pressure cell.

CONCLUSIONS

Physical modeling provides a useful link between theory and field-scale experiments. Using a physical model approach, we were able to measure changes in the acoustic response of pure fluids in the absence of a rock matrix in a nearly ideal setting.

Though we initially hoped to see a reflection amplitude response resulting from changes in pressure for both zero-offset and CMP data, we realized the change in velocity and density from the change in pressure was too small to observe an amplitude difference.

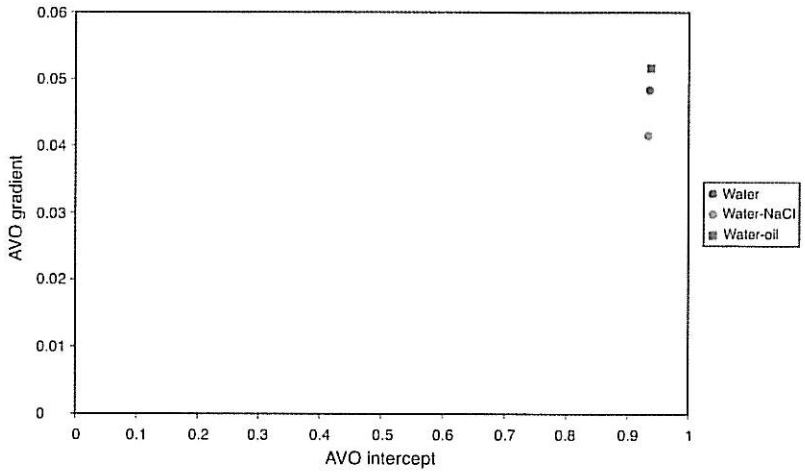

Figure 13. AVO crossplot of theoretical Zoepprtiz response to base of pressure cell reflection of fluids with known density and velocity.

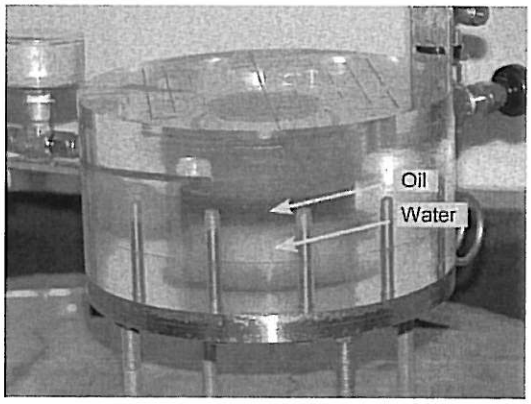

Figure 14. Separation between the oil and water in the pressure cell.

However, by crossplotting AVO intercept and gradient, we were able to detect differences in the AVO responses from the top and base reflections of a pressurized cell caused by changes in density and velocity of the contained fluids. Reflections from the top and base of the pressure cell showed a clear separation of AVO response between the fluid mixtures with and without oil. Dissolved CO_2 in the water-oil mixtures was undetectable, as was the addition of NaCl.

AVO response is useful to detect the contrast between pure water and a water-oil mixture, but is still unproven for detecting dissolved CO_2. Also, the base reflection, where the acoustic signal passed through the liquid mixture before and after reflection, showed better separation between the fluids than the top reflection. Even though the AVO intercept and gradient trends of the different fluids did not agree completely with the theoretical trends of the Zoeppritz response, there is still a clear separation in the AVO response from fluids that did not contain oil and those that did.

Our results show that AVO analysis may be useful for identifying changes in reservoir fluids.

ACKNOWLEDGMENTS

This work was partially supported by a grant from the Bureau of Educational and Cultural Affairs of the United States Department of State under the authority of the Fulbright-Hays Act of 1961, as amended, agreement no. PEPS-0262. We thank the Department of Exploration Geophysics at Curtin University for free access to their physical modeling facilities. We are grateful to Marvin Speece and Xiaobing Zhou for their helpful discussions. We thank Landmark Graphics Corporation, Veritas Hampson-Russell, and the CREWES project for providing software, and Sam Battah, director of NAR Engineering, for designing, building, and testing the physical model and helping with every aspect of the experiment. We also thank Damian Wandler at Colorado State University's Department of Statistics for his help with MANOVA.

REFERENCES

Batzle, M. L., D.-H. Han, and J. P. Castagna, 1995, Fluid effects on bright spot and AVO analysis: 65th Annual International Meeting, SEG, Expanded Abstracts, 1119–1121.

Batzle, M. L., D. Han, and R. Hofmann, 2001, Optimal hydrocarbon indicators: 71st Annual International Meeting, SEG, Expanded Abstracts, 1697–1700.

Batzle, M., and Z. Wang, 1992, Seismic properties of pore fluids: Geophysics, **57**, 1396–1408.

Castagna, J. P., 1993, AVO analysis — Tutorial and review, *in* J. P. Castagna and M. M. Backus, eds., Offset-dependent reflectivity — Theory and practice of AVO analysis: SEG, 3–36.

Davis, J. R., ed., 1990, Metals handbook: Properties and selection: Irons, steels, and high performance alloys, vol. 1, 10th ed.: ASM International.

Dix, C. H., 1955, Seismic velocities from surface measurements: Geophysics, **20**, 68–86.

Evans, B., 2004, Understanding fluid phase using a seismic PVT chamber: SPE Asia Pacific Oil and Gas Conference and Exhibition, SPE88517.

Foster, D., and R. Keys, 1999, Interpreting AVO responses: 69th Annual International Meeting, SEG, Expanded Abstracts, 748–751.

Harper, P., ed., 1975, Handbook of plastics and elastomers: McGraw-Hill Book Company.

Johnson, D. E., 1998, Applied multivariate methods for data analysts: Duxbury Press.

Landro, M., 2001, Discrimination between pressure and fluid saturation changes from time-lapse seismic data: Geophysics, **66**, 836–844.

Lide, D. R., ed., 2004, Handbook of chemistry and physics: CRC Press.

Lumley, D. E., 2001, The next wave in reservoir monitoring: The instrumented oil field: The Leading Edge, **20**, 640–648.

McIntire, P., ed., 1991, Nondestructive testing handbook: Ultrasonic testing, vol. 7, 2nd ed.: American Society for Nondestructive Testing.

Rutherford, S. R., and R. H. Williams, 1989, Amplitude-versus-offset variations in gas sands: Geophysics, **54**, 680–688.

Tura, A. C., and D. Lumley, 1999, Estimating pressure and saturation changes from time-lapse AVO data: 69th Annual International Meeting, SEG, Expanded Abstracts, 1655–1658.

Walden, A. T., 1991, Making AVO sections more robust: Geophysical Prospecting, **39**, 915–942.

Zoeppritz, K., 1919, Erdbebenwellen VIII B, Uber Reflexion and Durchgang Seismischer Wallen Durch Unstetigkeitsflachen: Gottinger Nachrichten I, 66–84.